Advances in Nano Research, *Vol. 19, No. 2 (2025) 185-200*
https://doi.org/10.12989/anr.2025.19.2.185

An analytical solution for vibration analysis of sandwich plates with auxetic core and functionally graded faces in a thermal environment

S. Chen* and J. Shi**

Department of Economic management, Leshan Normal University, Leshan, Sichuan, 614000, China

(*Received February 18, 2025, Revised August 13, 2025, Accepted August 19, 2025*)

Abstract. This study investigates the free vibration characteristics of rectangular sandwich plates that are partially supported by two-parameter elastic foundations, while also accounting for environmental temperature variations. The sandwich plate is constructed with an auxetic core layer, which exhibits a negative Poisson's ratio (NPR), complemented by two functionally graded (FG) face layers. The analysis considers the foundation's capacity to support the plate in either a complete or partial manner. Utilizing Hamilton's principle, the governing equations are derived based on a higher-order shear deformation theory framework. The application of this analytical method to the governing partial differential equations (PDEs) yields a system of algebraic equations. Solving this system in accordance with the specified boundary conditions results in an eigenvalue problem, which facilitates the determination of the natural frequencies of the plate. The findings of this study are validated against existing literature. Furthermore, the investigation explores the impact of various parameters including temperature fluctuations, characteristics of the auxetic core, boundary conditions, elastic foundation distribution patterns, and spring coefficients on the free vibration behavior of the sandwich plate. The results indicate that the auxetic core, characterized by its negative Poisson's ratio, confers metamaterial properties, thereby suggesting that the proposed model possesses significant potential for diverse engineering applications. In this analysis, higher-order shear deformation theory (HSDT) is employed to examine the free vibration characteristics of the sandwich plate, which features an auxetic core and functionally graded faces, while being subjected to a thermal medium and resting on a two-parameter elastic foundation. Given that the material properties of the NPR auxetic core layer are influenced by three geometric parameters, a thorough examination of the effective material properties is conducted, leading to the computation of the natural frequencies of the sandwich plate.

Keywords: analytical solution; boundary conditions; free vibration; NPR auxetic core; partially supported elastic foundation; sandwich plates; thermal medium

1. Introduction

In recent years, auxetic materials have attracted particular attention from researchers worldwide. Many researchers have studied auxetic materials due to their unusual mechanical behavior in the sports equipment, the electronics industry, the medical field, manufacturing, etc. Auxetic structures exhibit the largest effective Young's modulus which is at least one order higher than the other types of honeycomb core. Auxetic cores have a negative Poisson's ratio, and it can be adjusted with auxetic core parameters. This feature gives additional metamaterial properties, and thanks to this feature, they provide potential for use in hiding applications from sonar and radar waves (Wang *et al*. 2023). Wang *et al*. (2017) studied the dynamic characteristics of auxetic sandwich plates (ASPs) with asymmetrical metal honeycomb cores under explosive loads. Qi *et al*. (2017) assessed the blast resistance of ASPs with auxetic honeycomb cores for shock load mitigation. Various studies, including optimization of design parameters (Wang *et al*. 2018), energy absorption of 3D- printed structures (Sarvestani *et al*. 2018), and dynamic analysis using finite element methods (Tran *et al*. 2020), have been conducted on ASPs. Additionally, research on the nonlinear dynamics of sandwich structures (Nguyen and Pham, 2018), and the dynamic behavior of ASPs under different loading conditions (Hajmohammad *et al*. 2019) has been reported, highlighting their performance in various environments and applications. Recently, research on the static and dynamic responses of sandwich structures, specifically with an auxetic material/structure core, has increased continuously with their applications. Via TSDT, Natarajan and Manickam (2012) presented bending and vibration analysis of sandwich FGM plates. Alibeigloo and Alizadeh (2015) performed static and free vibration analysis of sandwich plates with FGM properties using the differential quadratic method (DQM). Shen *et al*. (2017) studied vibration of composite doubly curved shell resting in elastic foundation by higher order deformation theory (HSDT). Ghaznavi and Shariat (2019) researched the local and momentary changes of transverse deformations and stress components of a sandwich plate with an auxetic honeycomb core. According to TSDT Zhou *et al*. (2019) studied the vibration response of a sandwich plate with an auxetic core. Pham *et al*. (2020) investigated and analyzed the bending of a sandwich plate

*Corresponding author, Ph.D., Lecturer,
E-mail: 19181361823@163.com
**Co-corresponding author, Ph.D., Lecturer,
E-mail: LSSY198808@163.com

ISSN: 2287-237X (Print), 2287-2388 (Online)

with an auxetic aluminum core. TSDT and the finite element method (FEM) have been used to solve the equation of motion. In this research, all edges were considered as CCCC and SSSS. In framework of HSDT, Praveen *et al*. (2020) researched the response of free and forced vibrations behavior of sandwich plates with composite surfaces with a honeycomb core. FSDT and FEM with account of von Karman's geometric nonlinearity were utilized in this paper. Furthermore, the equations of motion were solved by utilizing Newton Raphson method at different boundary conditions, in the thermal environment. Chowdhary *et al*. (2021) studied the vibration behavior of sandwich GPLRC plates with honeycomb cores. Within the framework of an innovative quasi-3D shear deformation theory, Arshid *et al*. (2021) studied the vibrational behavior of a sandwich microplate with a FG core and piezoelectric face sheets using the Navier's solution approach. Singh and Harsha (2021) investigated the free vibration response of sandwich plates with honeycomb cores and FG platelets by means Navier's method. Jafari and Kiani (2021) used Navier solution to analysis free vibration of composite plates reinforced GPLs within the framework of a quasi-3D plate model. Based on FSDT, Kumar and Harsha (2021) studied the static and dynamic behavior of exponential FG piezoelectric materials under thermo-electro-mechanical loading. Based on FSDT, Kumar *et al*. (2021) investigated the free vibration of FGM plates with porosity on an elastic foundation using Galerkin method. Static and dynamic behavior of plain-woven composite plates without thickness periodicity was studied by Luo *et al*. (2021). Thang *et al*. (2022) investigated the bending and vibration analysis of a sandwich plate with an auxetic core and isotropic platelets with FG properties in the direction of thickness with the aids of FSDT and Navier solution. Vibration analysis of a composite sandwich panel in a hygrothermal environment in the framework of HSDT was conducted by Karimiasl and Alibeigloo (2022) using DQM. Khoddami Maraghi *et al*. (2022) used DQM to study the vibration and instability of a sandwich circular plate consisting of a magnetorheological fluid core. Utilizing the perturbation method, Karimiasl and Alibeigloo (2023) studied the nonlinear static and vibration characteristics of composite sandwich plate with honeycomb core with HSDT and modified couple stress theory. Namazinia *et al*. (2024) obtained the static response and natural frequencies of a sandwich plate in the hygrothermal environment with Reddy's TSDT. The plate consists of an auxetic core and Graphene platelet-reinforced composite (GPLRC) facing sheets. The equations of motion plate are obtained and solved by both Navier and the generalized DQM. Bennai *et al*. (2015) developed a new refined hyperbolic shear and normal deformation beam theory to study the free vibration and buckling of functionally graded (FG) sandwich beams under various boundary conditions. Bouchafa *et al*. (2015) used refined hyperbolic shear deformation theory (RHSDT) for the thermoelastic bending analysis of functionally graded sandwich plates. Tahouneh (2017) performed 3-D vibration analysis of MWCNT curved panels in FG-MWCNTs sandwich structures. Kormanikova *et al*. (2025) presented approaches for determining longitudinal Young's modulus of thin uni-directional CFRP composites. Wang *et al*. (2025) studied the effects of CNT waviness, aspect ratio, and damaged core on the vibrational behavior of FG nanocomposite sandwich beams on elastic foundations. Bouafia *et al*. (2021) studied Natural frequencies of FGM nanoplates embedded in an elastic medium. Khadir *et al*. (2021) investigated buckling and free vibration of functionally graded carbon nanotubes reinforced composite laminated nanoplates. The frequency characteristics, and sensitivity analysis of a size-dependent laminated composite cylindrical nanoshell under bi-directional thermal loading using Nonlocal Strain-stress Gradient Theory (NSGT) was studied by Dai *et al*. (2021). In another study, Ebrahimi *et al*. (2019) studied the frequency response of curved magneto-electro-viscoelastic functionally graded (CMEV-FG) nanobeams. Boutaleb *et al*. (2019) studied the dynamic response of the functionally graded rectangular nanoplates. Mohammed *et al*. (2024) study vibration of sandwich cylindrical shell with damaged core and FG face sheets resting on a two-parameter elastic foundation. In another study (Hatami *et al*. 2024) used an exact finite strip method for functionally graded-carbon nanotube sandwich plates to get the exact natural frequencies of the plates. Liu *et al*. (2024) study vibration of a composite cylindrical shell. The core of the shell is made of functionally graded (FG) porous materials and layers is fabricated of carbon nanotubes (CNTs) reinforced nanocomposites. Alnujaie *et al*. (2024) investigate free vibration response of plates, highlighting its potential to advance the understanding and application of material property variations in structural engineering. Shen *et al*. (2024) study free vibration analysis of FG porous spherical cap reinforced by graphene platelets resting on Winkler-type elastic foundation.

An elastic foundation reinforcement can significantly enhance the stiffness of a structure. In engineering practice, structures are usually only locally supported by elastic foundations, giving rise to the concept of the partially supported elastic foundation (PSEF) have potential applications. The plates supported on partial foundations have been considered for vibration analysis by researchers. For instance, Motaghian *et al*. (2012) studied the free vibration characteristics of rectangular plates on specific regions of elastic foundations. Jahromi *et al*. (2013) employed the generalized differential quadrature (GDQ) method to study the free vibration of a rectangular plate resting on PSEF with Pasternak type. Kim (2015) investigated the vibration response of a FG cylindrical shell partly supported by a Pasternak elastic foundation. Shahbaztabar and Arteshyar (2019) considered the buckling response of FG plates partially on an elastic foundation with the differential quadrature element method. Moraveji Tabasi *et al*. (2020) extended the ES-MITC3 element based on first-order shear deformation theory (FSDT) for the free vibration analysis of FG plates resting on the partially supported elastic foundation. Nguyen *et al*. (2022) examined buckling and free vibration analysis of fiber metal-laminated plates on a total and partial elastic foundation. However, these studies on localized elastic foundations typically involve complex numerical techniques. Recently, Hoang *et al*. (2024) proposed a simpler analytical

method based on Galerkin's method to identify the location of localized elastic bases through straightforward integration, eliminating the need for complex algorithms. Ameer *et al*. (2024) studied free vibration behavior of trapezoidal shaped coupled double-layered graphene sheets (DLGS) system using first-order shear deformation theory (FSDT) and incorporating nonlocal elasticity theory. Barka *et al*. (2016) studied thermal post-buckling behavior of imperfect temperature-dependent sandwich FGM plates resting on Pasternak elastic foundation. Park *et al*. (2016) used modified couple stress based third-order shear deformation theory for dynamic analysis of sigmoid functionally graded materials (S-FGM) plates. Bhatti *et al*. (2023) study the behavior of hybrid nanofluid flow using a model based on third-grade sodium alginate. Sodium alginate has the potential to be used in the extraction of geothermal energy. The investigation of the reflection issue in a hygrothermal medium in nonlocal elasticity conducted by Yadav *et al*. (2024). Arefi (2015) suggested an analytical solution of a curved beam with different shapes made of functionally graded materials (FGMs). Abo-Dahab *et al*. (2020) used the generalized thermoelasticity theory, with one thermal relaxation time (TR), to examine the thermoelastic problem of a functionally graded thin slim strip (TSS). Bouguenina *et al*. (2015) studied FG plates with variable thickness subjected to thermal buckling. Hosseini and Zhang (2018) considered wave propagation analysis in a FG Graphene platelets-reinforced nano-composite cylinder. Marin (2010) considered a right cylinder composed of a physically dipolar thermoelastic material for which one plane end was subjected to an excitation which is harmonic in time. Marin *et al*. (2022) used a linear theory for the thermoelasticity of type III for Cosserat media. Marin *et al*. (2014) have tried to extend the domain of influence result to cover the micropolar thermo-elastic diffusion. Tahouneh *et al*. (2019) used trimming technique to create the cutout in geometry of L-shape plate. Tahouneh *et al*. (2020) studied vibration of vacancy defected graphene sheet as a nonisotropic structure via molecular dynamic and continuum approaches. Tornabene (2009) used four-parameter power-law distribution to study the dynamic behavior of moderately thick functionally graded conical and cylindrical shells. Tornabene and Ceruti (2013) studied a mixed static and dynamic optimization of four-parameter functionally graded material (FGM) doubly curved shells and panels. Tornabene *et al*. (2014) studied free vibration of free-form doubly-curved shells made of functionally graded materials using higher-order equivalent single layer theories.

The review highlights that auxetic core layers are commonly used in sandwich structures due to their advantages, such as high damping, impact absorption, and fracture resistance. FGM materials have also gained significant attention for their properties, making them suitable for developing adaptive structures. Combining these two materials in sandwich configurations can provide unique mechanical properties for various applications. However, research on sandwich structures with auxetic cores and FGM surfaces is still limited. Therefore, studying the vibration of these sandwich plates is essential to deepen our understanding of their mechanical behavior. The vibration analysis of the existing sandwich plate with a metamaterial property will be presented for the first time subjected to temperature change and partially supported elastic foundation.

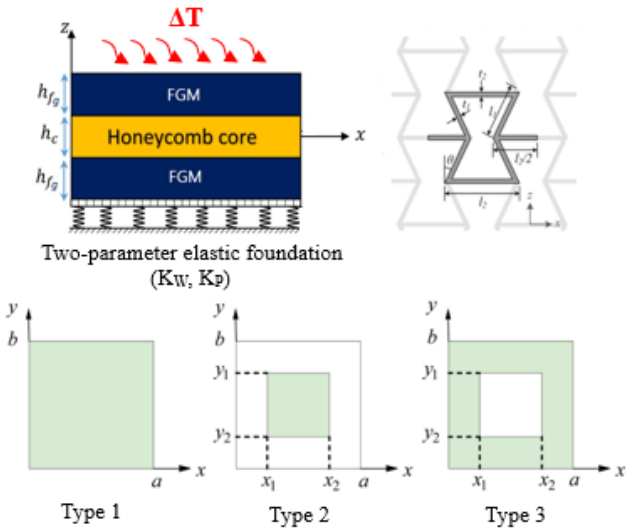

Fig. 1 Schematic view of the sandwich plate with auxetic core, resting on PSEF

2. Theory and formulation

2.1 Sandwich plate with auxetic core

In this study, we consider a smart sandwich plate with two FGM layers, an auxetic core layer, which has length *a*, width *b*, and total thickness *h* as illustrated in Fig. 1, resting on PSEF. *x* and *y* are in-plane axes located at the middle layer of the auxetic core, and z is the direction that extends along the thickness of the plate. h_c and h_{fg} are the thicknesses of core layer and FG layer, respectively. Also, the top surface subjected to temperature rise (ΔT). Figure 1b demonstrates three typical distribution patterns of foundations, where the colorful parts are the distribution zones of substrate. The various distribution patterns of elastic foundations are characterized by the coordinates of points on the *x* and *y* axes *xi* and *yi* . (i=1,2).

The core layer of the proposed sandwich plate is made of an auxetic material with NPR. The auxetic core layer consists of honeycomb cells placed in a systematic way, where θ, l_2, l_1, and $t_1=t_3$ represent the angle of inclination, the length of the horizontal wall, the length of the inclined cell wall, and the thickness of the cell wall, respectively. The material properties such as young modulus (E), shear modulus (G), Poisson's ratio (ν), thermal expansion coefficients ($\alpha^C{}_{11}$) and density (ρ) of the auxetic core can be expressed using the following equations (Zhu *et al*. 2019, Ha *et al*. 2022):

$$E_{11}^{C} = E_M \left[\frac{(\beta_1 - \sin\theta)\beta_3^3}{[(\beta_1 \sec^2(\theta) + \tan^2(\theta))\beta_3^2 + 1]\cos^3(\theta)} \right] \quad (1)$$

$$E_{22}^{C} = E_M\left[\frac{\beta_3^3}{(\beta_3^2+\tan^2(\theta))(\cos(\theta)\beta_1-\cos(\theta)\sin(\theta))}\right]$$

$$G_{12}^{C} = G_M\left[\frac{\beta_3^3}{(2\beta_1^2+\beta_1)\cos\theta}\right]$$

$$G_{13}^{C} = G_M\left[\frac{2\sin^2(\theta)+\beta_1}{2(\beta_1-\sin(\theta))}+\frac{-\sin(\theta)+\beta_1}{2\beta_1+1}\right]\frac{\beta_3}{2\cos(\theta)}$$

$$\rho^{c} = \rho_M\left[\frac{(2+\beta_1)\beta_3}{2(\beta_1-\sin(\theta))\cos(\theta)}\right]$$

$$\alpha_{11}^{C} = \alpha_M\frac{\beta_3\cos(\theta)}{\beta_1+\sin(\theta)}$$

$$v_{12}^{C} = \frac{(\sin(\theta)-\beta_1)(\sin(\theta))(1-\beta_3^2)}{\cos^2(\theta)[\beta_3^2(\beta_1\sec^2(\theta)+\tan^2(\theta))+1]}$$

In which $\beta_1 = l_2/l_1$ and $\beta_3 = t_1/l_1$. Also, the superscript *c* and subscript *M* represent the core layer and metallic material, respectively. θ is the inclined angle which is in the range $\theta < \arcsin(\frac{\beta_1}{2})$. Figures (2a-2d) shows the effect of the parameter β_3 and inclined angle θ on the density and Elastic moduli of auxetic core made of SUS304, respectively. As shown in the Figs. (2a, 2b) as the β_3 parameter increases for any fixed value of θ, the ρ and E_{11} value rises too. Besides, with the increase in the inclined angle θ for any β_3, the density and Elastic moduli in the x direction increases, too. As shown in the Fig.3 (a-d), Poisson's ratios of auxetic core in different directions are functions of geometrical parameters of core's cell. The NPR can be modified in the xy and yx directions and thus the Shear moduli can be adjusted.

On the other hand, the material properties of power-law FG layers are defined as:

$$P = P_m + (P_c - P_m)\left(z-\frac{h_c}{2}\right)^p;\ \frac{h_c}{2} \le z \le \frac{h_c}{2}+h_{fg}$$
$$P = P_m + (P_c - P_m)\left(-z-\frac{h_c}{2}\right)^p;\ \frac{-h_c}{2}-h_{fg} \le z \le -\frac{h_c}{2} \quad (2)$$

In which the parameter P represents the power index of FG layers.

2.2 Temperature field on the sandwich plate

In the presence of a nonlinear temperature increase (NLTR) across the thickness direction of the plates, the one-dimensional heat transfer problem given below can be addressed with specific temperature boundary limits to figure out the upper and lower surface temperatures of the plate. The temperature field assumed to be uniform over the plate surfaces and varying along the thickness of the plate due to heat conduction. In such a case, the temperature variation along the plate thickness can be obtained by solving the steady-state heat transfer equation as (Daikh *et al*. 2019, Daikh and Megueni, 2018):

$$-\frac{d}{dz}\left(K(z)\frac{dT(z)}{dz}\right) = 0 \quad (3)$$

The temperature boundary is: $T(-h_{fg}-h_c/2) = T_b$ at the bottom surface and $T(h_{fg}+h_c/2)=T_t$ at top surface, in which $T_t=T_b+\Delta T$. The temperature distribution of sandwich plate is obtained as (Daikh *et al*. 2019, Daikh and Megueni, 2018):

$$T(z) = T_b + \Delta T\frac{\int_{-h_{fg}-h_c/2}^{z}k(z)dz}{\int_{-h_{fg}-h_c/2}^{h_{fg}+h_c/2}\frac{dz}{k(z)}} \quad (4)$$

Here, *k*(z) denotes the thermal conductivity coefficient.

2.3 Kinematical formulations

Based on the higher-order shear deformation theory, the displacement field of the plate at any point, in terms of mid-plane displacements through x- and y-axes (u and v, respectively), bending and shear components of transverse displacement of the midplane (w_b and w_s, respectively), and the time expression (t), can be assumed by Jung *et al*. (2016):

$$u_1(x,y,z,t) = u(x,y,t) - z\frac{\partial w_b}{\partial x} - f(z)\frac{\partial w_s}{\partial x},$$
$$u_2(x,y,z,t) = v(x,y,t) - z\frac{\partial w_b}{\partial y} - f(z)\frac{\partial w_s}{\partial y}, \quad (5)$$
$$u_3(x,y,z,t) = w_b(x,y,t) + w_s(x,y,t)$$

In which $(z) = z - \frac{h}{\pi}\,sin\left(\frac{\pi z}{h}\right)$, is the shear stress distribution function through the sandwich plate's thickness. Nonzero strains of the four-variable plate model are defined as:

$$\begin{Bmatrix}\varepsilon_x\\ \varepsilon_y\\ \gamma_{xy}\end{Bmatrix} = \begin{Bmatrix}\varepsilon_x^0\\ \varepsilon_y^0\\ \gamma_{xy}^0\end{Bmatrix} + z\begin{Bmatrix}\kappa_x^b\\ \kappa_y^b\\ \kappa_{xy}^b\end{Bmatrix} + f\begin{Bmatrix}\kappa_x^s\\ \kappa_y^s\\ \kappa_{xy}^s\end{Bmatrix};$$
$$\begin{Bmatrix}\gamma_{yz}\\ \gamma_{xz}\end{Bmatrix} = g\begin{Bmatrix}\gamma_{yz}^s\\ \gamma_{xz}^s\end{Bmatrix} \quad (6)$$

wWhere $= 1 - \frac{\partial f}{\partial z}$, and:

$$\begin{Bmatrix}\varepsilon_x^0\\ \varepsilon_y^0\\ \gamma_{xy}^0\end{Bmatrix} = \begin{Bmatrix}\partial_x u\\ \partial_y v\\ \partial_y u+\partial_x v\end{Bmatrix};\begin{Bmatrix}\kappa_x^b\\ \kappa_y^b\\ \kappa_{xy}^b\end{Bmatrix} = \begin{Bmatrix}-\partial_{xx}w_b\\ -\partial_{yy}w_b\\ -2\partial_{xy}w_b\end{Bmatrix},$$
$$\begin{Bmatrix}\kappa_x^s\\ \kappa_y^s\\ \kappa_{xy}^s\end{Bmatrix} = \begin{Bmatrix}-\partial_{xx}w_s\\ -\partial_{yy}w_s\\ -2\partial_{xy}w_s\end{Bmatrix};\begin{Bmatrix}\gamma_{yz}^s\\ \gamma_{xz}^s\end{Bmatrix} = \begin{Bmatrix}\partial_y w_s\\ \partial_x w_s\end{Bmatrix} \quad (7)$$

3. Hamilton principle

Employing the Hamilton's principle, the motion equation could be decided by as follows in terms of strain and kinetic energies (Π_S and Π_K, respectively), and external forces' work (Π_W) (Zhang *et al*. 2022):

$$\int_0^t \delta(\Pi_s - \Pi_k + \Pi_W + U_F)dt = 0 \quad (8)$$

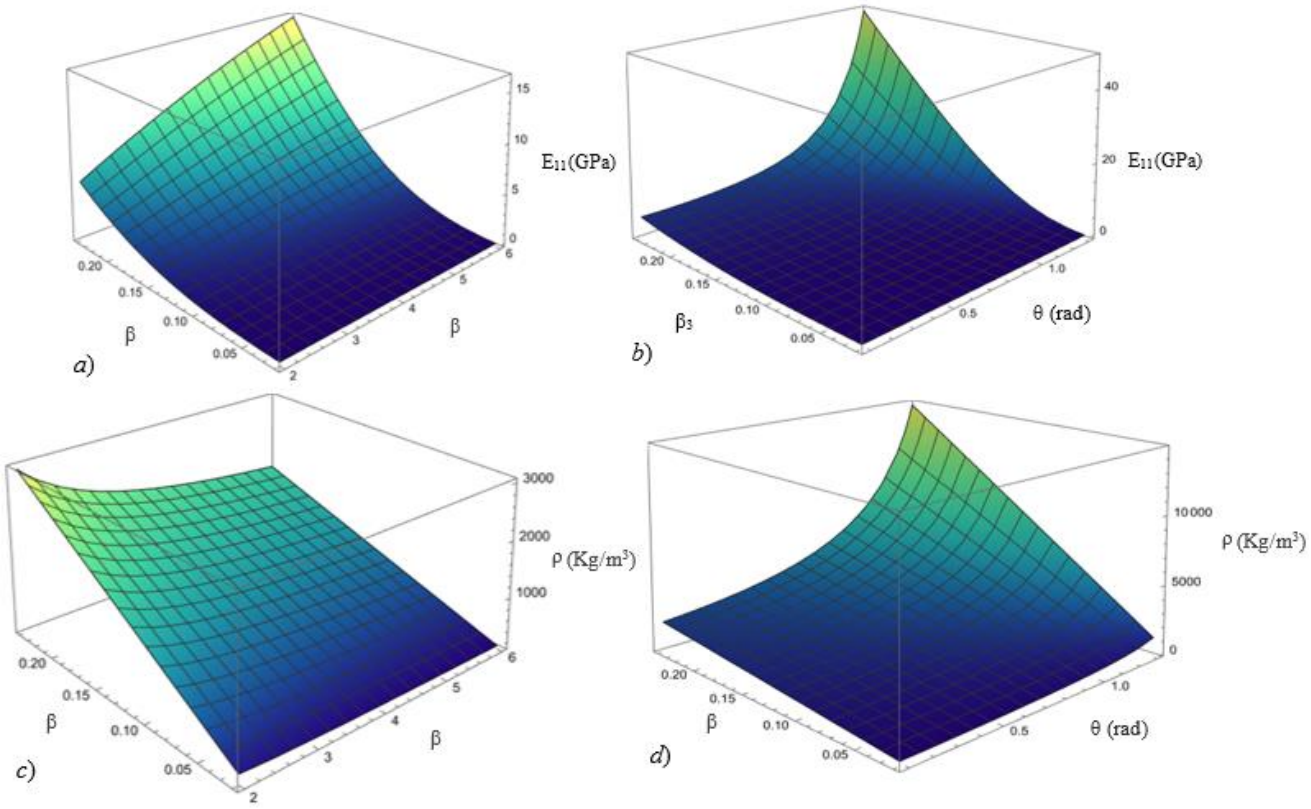

Fig. 2 Variation of density and Elastic moduli of auxetic core versus the geometrical parameters of auxetic layer; (a) $E_{11}(\beta_1, \beta_3)$, (b) $E_{11}(\theta, \beta_3)$, (c)$\rho(\beta_1, \beta_3)$, (d) $\rho(\theta, \beta_3)$

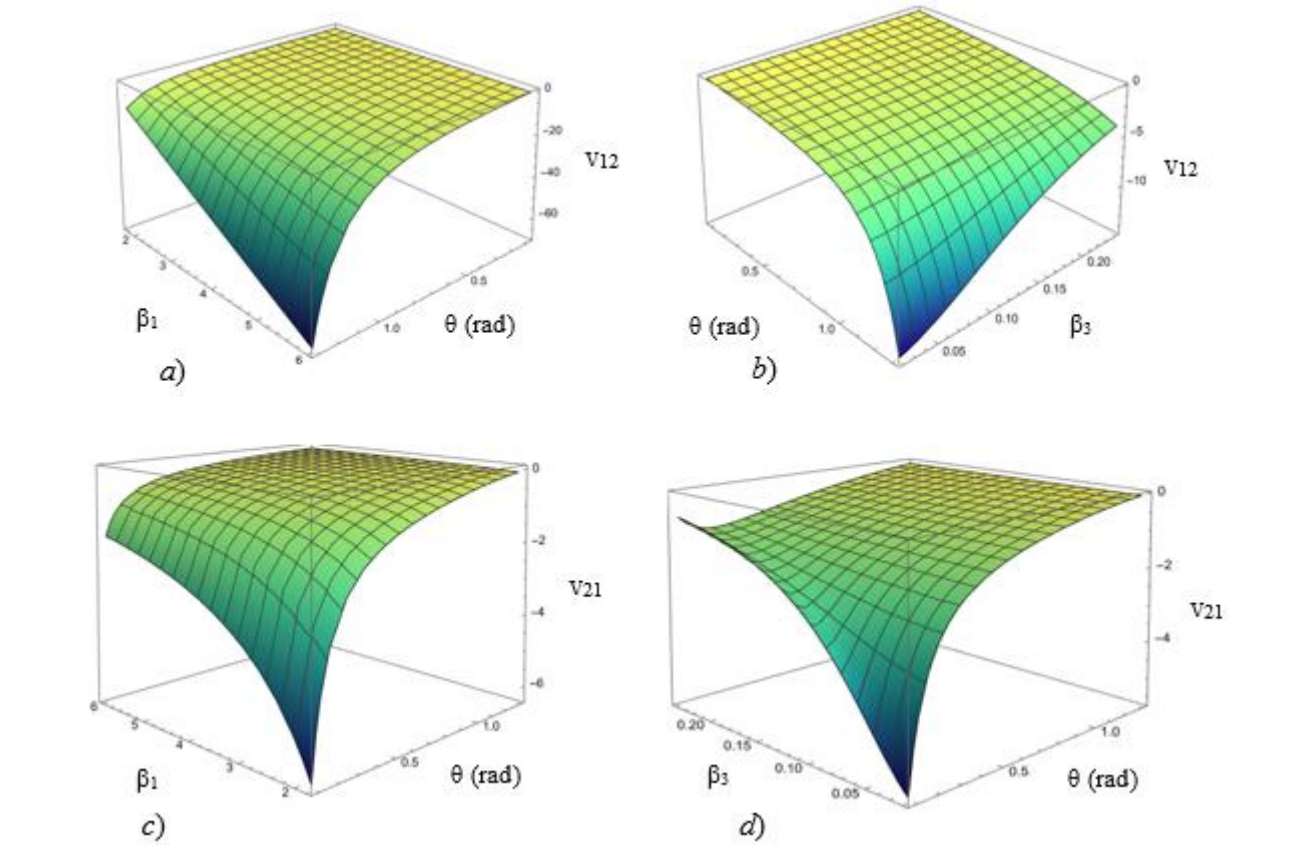

Fig. 3 Variation of Poisson's ratios of auxetic core in different directions versus the geometrical parameters of auxetic layer; (a) $v_{12}(\beta_1, \theta)$, (b) $v_{12}(\theta, \beta_3)$, (c) $v_{21}(\beta_1, \theta)$, (d) $v_{21}(\theta, \beta_3)$

The virtual strain energy variation can be stated as:

$$\begin{aligned}\delta\Pi_s &= \int_v \sigma_{ij}\delta\varepsilon_{ij}\,dV \\ &= \int_v \begin{pmatrix}\sigma_x\delta\varepsilon_x + \sigma_y\delta\varepsilon_y + \sigma_{xy}\delta\gamma_{xy} \\ +\sigma_{yz}\delta\gamma_{yz} + \sigma_{xz}\delta\gamma_{xz}\end{pmatrix} dV\end{aligned} \tag{9}$$

$$\delta\Pi_s = \int_0^l \begin{bmatrix} N_x\dfrac{\partial\delta u}{\partial x} - M_x^b\dfrac{\partial^2\delta w_b}{\partial x^2} - M_x^s\dfrac{\partial^2\delta w_s}{\partial x^2} \\ +N_y\dfrac{\partial\delta v}{\partial y} - M_y^b\dfrac{\partial^2\delta w_b}{\partial y^2} - M_y^s\dfrac{\partial^2\delta w_s}{\partial y^2} \\ +N_{xy}\left(\dfrac{\partial\delta u}{\partial y} + \dfrac{\partial\delta v}{\partial x}\right) - 2M_{xy}^b\dfrac{\partial^2\delta w_b}{\partial x\partial y} \\ -2M_{xy}^s\dfrac{\partial^2\delta w_s}{\partial x\partial y} + Q_{yz}\dfrac{\partial\delta w_s}{\partial y} + Q_{xz}\dfrac{\partial\delta w_s}{\partial x}\end{bmatrix} dx \tag{10}$$

In which the stress variables can be defined by:

$$\begin{aligned}\left(N_i, M_i^b, M_i^s\right) &= \int_A (1, z, f)\sigma_i\,dA \quad ; i = (x, y, xy) \\ Q_i &= \int_A g\sigma_i\,dA \quad ; i = (xz, yz)\end{aligned} \tag{11}$$

The variation of externally applied N_x^0, N_y^0, and N_{xy}^0 in-plane forces work can be penned in the subsequent form:

$$\delta\Pi_W = \int_0^l \begin{pmatrix} N_x^0\dfrac{\partial(w_b+w_s)}{\partial x}\dfrac{\partial\delta(w_b+w_s)}{\partial x} + \\ N_y^0\dfrac{\partial(w_b+w_s)}{\partial y}\dfrac{\partial\delta(w_b+w_s)}{\partial y} + \\ 2\delta N_{xy}^0\dfrac{\partial(w_b+w_s)}{\partial x}\dfrac{\partial(w_b+w_s)}{\partial y}\end{pmatrix} dxdy \tag{12}$$

The variation of work done by partially elastic foundation with surface A_f equals to:

$$\delta U_F = \int_{A_f} \begin{bmatrix} \bar{k}_W(w_b+w_s)\delta(w_b+w_s) + \\ \bar{k}_P\begin{pmatrix}\dfrac{\partial(w_b+w_s)}{\partial x}\dfrac{\partial\delta(w_b+w_s)}{\partial x} + \\ \dfrac{\partial(w_b+w_s)}{\partial y}\dfrac{\partial\delta(w_b+w_s)}{\partial y}\end{pmatrix}\end{bmatrix} dxdy \tag{13}$$

The detailed variation of the integration on different PSEF is given in Appendix A. The virtual kinetic energy variation of the plate can be described as:

$$\begin{aligned} &A_{66}\frac{\partial^2 v}{\partial x^2} + A_{22}\frac{\partial^2 v}{\partial y^2} + (A_{12}+A_{66})\frac{\partial^2 u}{\partial x\partial y} \\ &-B_{22}\frac{\partial^3 w_b}{\partial y^3} - (B_{12}+2B_{66})\frac{\partial^3 w_b}{\partial x^2\partial y} \\ &-B_{22}^s\frac{\partial^3 w_s}{\partial y^3} - (B_{12}^s+2B_{66}^s)\frac{\partial^3 w_s}{\partial x^2\partial y} \\ &\left(-I_0\frac{\partial^2 v}{\partial t^2} + I_1\frac{\partial^3 w_b}{\partial y\partial t^2} + J_1\frac{\partial^3 w_s}{\partial y\partial t^2}\right) = 0\end{aligned} \tag{14}$$

Where the I_0, I_1, J_1, I_2, J_2 and J_3 are mass moments of inertias, and equals to:

$$(I_0, I_1, J_1, I_2, J_2, J_3) = \int_{-h/2}^{h/2} (1, z, f, z^2, zf, f^2)\rho(z)dz \tag{15}$$

The coupled equations are obtained by substituting Eq. (10) and Eqs. (12-14) into Eq. (8), while the δu, δv, δw_b, δw_s and $\delta\varphi$ coefficients are all zero:

$$\frac{\partial N_x}{\partial x} + \frac{\partial N_{xy}}{\partial y} = I_0\frac{\partial^2 u}{\partial t^2} - I_1\frac{\partial^3 w_b}{\partial x\partial t^2} - J_1\frac{\partial^3 w_s}{\partial x\partial t^2} \tag{16a}$$

$$\frac{\partial N_{xy}}{\partial x} + \frac{\partial N_y}{\partial y} = I_0\frac{\partial^2 v}{\partial t^2} - I_1\frac{\partial^3 w_b}{\partial y\partial t^2} - J_1\frac{\partial^3 w_s}{\partial y\partial t^2} \tag{16b}$$

$$\begin{aligned} &\frac{\partial^2 M_x^b}{\partial x^2} + 2\frac{\partial^2 M_{xy}^b}{\partial x\partial y} + \frac{\partial^2 M_y^b}{\partial y^2} - N^E\nabla^2(w_b+w_s) \\ &+\bar{k}_W(w_b+w_s) - \bar{k}_P\nabla^2(w_b+w_s) = \\ &I_0\frac{\partial^2(w_b+w_s)}{\partial t^2} + I_1\left(\frac{\partial^3 u}{\partial x\partial t^2} + \frac{\partial^3 v}{\partial y\partial t^2}\right) \\ &-I_2\nabla^2\left(\frac{\partial^2 w_b}{\partial t^2}\right) - J_2\nabla^2\left(\frac{\partial^2 w_s}{\partial t^2}\right)\end{aligned} \tag{16c}$$

$$\begin{aligned} &-\frac{\partial^2 M_x^s}{\partial x^2} + 2\frac{\partial^2 M_{xy}^s}{\partial x\partial y} + \frac{\partial^2 M_y^s}{\partial y^2} + \frac{\partial Q_{xz}}{\partial x} + \\ &\frac{\partial Q_{yz}}{\partial y} - N^E\nabla^2(w_b+w_s) + \bar{k}_W(w_b+w_s) \\ &-\bar{k}_P\nabla^2(w_b+w_s) = J_1\left(\frac{\partial^3 u}{\partial x\partial t^2} + \frac{\partial^3 v}{\partial y\partial t^2}\right) \\ &-J_2\nabla^2\left(\frac{\partial^2 w_b}{\partial t^2}\right) - J_3\nabla^2\left(\frac{\partial^2 w_s}{\partial t^2}\right)\end{aligned} \tag{16d}$$

The stress-strain relations for each layer of sandwich plate subjected to the thermo-mechanical loads can be organized as:

$$\begin{aligned} &\sigma_{xx} = \left(\tilde{c}_{11}\varepsilon_{xx} + \tilde{c}_{12}\varepsilon_{yy} - \tilde{\beta}_1\Delta T\right) \\ &\sigma_{yy} = \left(\tilde{c}_{12}\varepsilon_{xx} + \tilde{c}_{11}\varepsilon_{yy} - \tilde{\beta}_1\Delta T\right);\ \sigma_{xy} = \tilde{c}_{66}\gamma_{xy} \\ &\sigma_{xz} = \left(\tilde{c}_{55}\gamma_{xz}E_x - \tilde{\beta}_1\Delta T\right);\ \sigma_{yz} = \left(\tilde{c}_{55}\gamma_{yz} - \tilde{\beta}_1\Delta T\right)\end{aligned} \tag{17}$$

In which, $\tilde{c}_{ij}$ represent the elastic stiffness coefficients for the plane stress and $\tilde{\beta}_1$ is thermo-elastic coupling coefficients equals to: $\tilde{c}_{11} = c_{11} - \frac{c_{13}^2}{c_{33}}$; $\tilde{c}_{12} = c_{12} - \frac{c_{13}^2}{c_{33}}$; $\tilde{c}_{66} = c_{66}$.

Integrating Eq. (17) for the cross-section of plate, the force-strain and the moment-strain relations can be reached for the sandwich plate, showing by detail in the Appendix B. Finally, the coupled governing equations regarding the displacements for the refined four-variable shear deformation of the plate can be obtained by replacing Eqs. (B1)-(B4) from Appendix B, into Eqs. (16a)-(16d) in the next relations as:

$$\begin{aligned} &A_{11}\frac{\partial^2 u}{\partial x^2} + A_{66}\frac{\partial^2 u}{\partial y^2} + (A_{12}+A_{66}) \\ &\frac{\partial^2 v}{\partial x\partial y} - B_{11}\frac{\partial^3 w_b}{\partial x^3} - (B_{12}+2B_{66})\frac{\partial^3 w_b}{\partial x\partial y^2} \\ &-B_{11}^s\frac{\partial^3 w_s}{\partial x^3} - (B_{12}^s+2B_{66}^s)\frac{\partial^3 w_s}{\partial x\partial y^2} + \\ &\left(-I_0\frac{\partial^2 u}{\partial t^2} + I_1\frac{\partial^3 w_b}{\partial x\partial t^2} + J_1\frac{\partial^3 w_s}{\partial x\partial t^2}\right) = 0\end{aligned} \tag{18a}$$

$$
\begin{aligned}
&A_{66}\frac{\partial^2 v}{\partial x^2}+A_{22}\frac{\partial^2 v}{\partial y^2}+(A_{12}+A_{66})\frac{\partial^2 u}{\partial x\partial y}\\
&-B_{22}\frac{\partial^3 w_b}{\partial y^3}-(B_{12}+2B_{66})\frac{\partial^3 w_b}{\partial x^2\partial y}\\
&-B^s_{22}\frac{\partial^3 w_s}{\partial y^3}-(B^s_{12}+2B^s_{66})\frac{\partial^3 w_s}{\partial x^2\partial y}\\
&\left(-I_0\frac{\partial^2 v}{\partial t^2}+I_1\frac{\partial^3 w_b}{\partial y\partial t^2}+J_1\frac{\partial^3 w_s}{\partial y\partial t^2}\right)=0
\end{aligned}
\tag{18b}
$$

$$
\begin{aligned}
&B_{11}\frac{\partial^3 u}{\partial x^3}+\left(B_{12}+2B_{66}\right)\frac{\partial^3 u}{\partial x\partial y^2}+\\
&\left(B_{12}+2B_{66}\right)\frac{\partial^3 v}{\partial x^2\partial y}+B_{22}\frac{\partial^3 v}{\partial y^3}\\
&-D_{11}\frac{\partial^4 w_b}{\partial x^4}-2\left(D_{12}+2D_{66}\right)\frac{\partial^4 w_b}{\partial x^2\partial y^2}\\
&-D_{22}\frac{\partial^4 w_b}{\partial y^4}-D^s_{11}\frac{\partial^4 w_s}{\partial x^4}-\\
&2\left(D^s_{12}+2D^s_{66}\right)\frac{\partial^4 w_s}{\partial x^2\partial y^2}-D^s_{22}\frac{\partial^4 w_s}{\partial y^4}+\\
&-I_0\frac{\partial^2\left(w_b+w_s\right)}{\partial t^2}-I_1\left(\frac{\partial^3 u}{\partial x\partial t^2}+\frac{\partial^3 v}{\partial y\partial t^2}\right)+\\
&I_2\nabla^2\left(\frac{\partial^2 w_b}{\partial t^2}\right)+J_2\nabla^2\left(\frac{\partial^2 w_s}{\partial t^2}\right)+\\
&\bar{k}_w\left(w_b+w_s\right)-\left(N^T-\bar{k}_p\right)\nabla^2\left(w_b+w_s\right)=0
\end{aligned}
\tag{18c}
$$

$$
\begin{aligned}
&B^s_{11}\frac{\partial^3 u}{\partial x^3}+\left(B^s_{12}+2B^s_{66}\right)\frac{\partial^3 u}{\partial x\partial y^2}+\\
&\left(B^s_{12}+2B^s_{66}\right)\frac{\partial^3 v}{\partial x^2\partial y}+B^s_{22}\frac{\partial^3 v}{\partial y^3}\\
&-D^s_{11}\frac{\partial^4 w_b}{\partial x^4}+A^s_{55}\frac{\partial^2 w_s}{\partial x^2}+A^s_{44}\frac{\partial^2 w_s}{\partial y^2}\\
&-2\left(D^s_{12}+2D^s_{66}\right)\frac{\partial^4 w_b}{\partial x^2\partial y^2}\\
&-D^s_{22}\frac{\partial^4 w_b}{\partial y^4}-H^s_{11}\frac{\partial^4 w_s}{\partial x^4}-\\
&2\left(H^s_{12}+2H^s_{66}\right)\frac{\partial^4 w_s}{\partial x^2\partial y^2}-H^s_{22}\frac{\partial^4 w_s}{\partial y^4}-\\
&I_0\frac{\partial^2\left(w_b+w_s\right)}{\partial t^2}-J_1\left(\frac{\partial^3 u}{\partial x\partial t^2}+\frac{\partial^3 v}{\partial y\partial t^2}\right)\\
&+J_2\nabla^2\left(\frac{\partial^2 w_b}{\partial t^2}\right)+J_3\nabla^2\left(\frac{\partial^2 w_s}{\partial t^2}\right)+\bar{k}_w\left(w_b+w_s\right)\\
&-\left(N^T-\bar{k}_p\right)\nabla^2\left(w_b+w_s\right)=0
\end{aligned}
\tag{18d}
$$

4. Solution method

Considering different boundary conditions, the displacement where satisfy the boundary condition, in the form of unknown coefficients ($\overline{u_{mn}}$ $\overline{v_{mn}}$ $\overline{w_{b_{mn}}}$ $\overline{w_{s_{mn}}}$) and trigonometric functions are expressed as (Arani *et al*. 2018):

$$
\begin{pmatrix} u\\ v\\ w_b\\ w_s \end{pmatrix}=\sum_{m=1}^{\infty}\sum_{n=1}^{\infty}\begin{pmatrix} \overline{u_{mn}}\frac{d}{dx}X_m(x)Y_n(y)\\ \overline{v_{mn}}X_m(x)\frac{d}{dy}Y_n(y)\\ \overline{w_{b\,mn}}X_m(x)Y_n(y)\\ \overline{w_{s\,mn}}X_m(x)Y_n(y) \end{pmatrix}e^{i\Omega_{mn}t} \tag{19}
$$

Where Ω_{mn} is the natural frequency. The functions $X_m(x), Y_n(y)$ depends on boundary condition of plate in the x, y directions, respectively; and can be written as (Arani *et al*. 2018):

$$
\begin{aligned}
X_m(x)&=\sin(\Omega_m x)+\zeta_m\cos(\Omega_m x)\\
&+\eta_m\sinh(\Omega_m x)+\xi_m cosh(\Omega_m x)\\
Y_n(y)&=\sin(\Omega_n y)+\zeta_n\cos(\Omega_n y)\\
&+\eta_n\sinh(\Omega_n y)+\xi_n cosh(\Omega_n y)
\end{aligned}
\tag{20}
$$

These constant coefficients are defined in Table 1 for different boundary conditions. Substituting Eq. (19) and Eq. (20) into Eqs. (18a-18d), the final relation for free vibration problem is obtained in the matrix form as:

$$([K]-\Omega^2[M])\{\Delta\}=\{0\} \tag{21}$$

In which $\{\Delta\}=(\overline{u_{mn}}\ \ \overline{v_{mn}}\ \ \overline{w_{b_{mn}}}\ \ \overline{w_{s_{mn}}})$. Also, [K] and [M] are stiffness and inertia matrices, which are not presented here to avoid the length of the text. Finally, the natural frequencies of the system can be obtained by solving the eigenvalue equation $|[K]-\Omega^2[M]|=0$.

5. Results and discussion

5.1 Validation of the method

For the first case, the first and second dimensionless natural frequencies ($\bar{\Omega}=\Omega\frac{a^2}{h}\sqrt{\frac{\rho_m}{E_m}}$) of isotropic plates partially supported by an elastic foundation parallel to the plate edges, similar to type 2 in which x_1=a/3, x_2=5a/6, y_1=b/4, y_2 =7b/8 ; validated by numerical results of Motaghian *et al*. (2012), Jahromi *et al*. (2013) and Nguyen *et al*. (2022) for various boundary condition and substrate Winkler stiffness (K_W) at Tables 2(a) and (2b). Physical and Geometrical Parameters of isotropic plate are: a/h=20, b/a=0.5, h=10cm, E_m=200GPa and ρ_m=7.85g/cm^3. The similarity between the results reveals the accuracy and reliability of the model in calculating the frequency of the sandwich plates.

As another example, square three-layer SSSS sandwich plates with the auxetic core layer and isotropic faces have been considered, resting on Elastic Foundation (EF) with Winkler stiffness K_w and shear stiffness K_p. All layers are isotropic and made by aluminum, also the geometrical parameters of the core layer are θ, β_1 and β_3=0.01385

The first natural frequencies with different values of the EF parameter and geometrical parameters of the core layer are presented in Table 3 and validated by numerical results

Table 1 Coefficients of Eq. (20) for various boundary conditions

B.C.	Ω_r	ζ_r	η_r	ξ_r
SS	$r\pi$	0	0	0
SC	$(4r+1)\pi/4$	0	$-\frac{\sin(\Omega_r)}{\sinh(\Omega_r)}$	0
CC	$(2r+1)\pi/2$	$-\frac{sin(\Omega_r)-sinh(\Omega_r)}{\cos(\Omega_r)-cosh(\Omega_r)}$	-1	$-\zeta_r$
CF	$(2r-1)\pi/4$	$-\frac{sin(\Omega_r)+sinh(\Omega_r)}{\cos(\Omega_r)+cosh(\Omega_r)}$	-1	$-\zeta_r$
FF	$(2r+1)\pi/2$	$-\frac{sin(\Omega_r)-sinh(\Omega_r)}{\cos(\Omega_r)-cosh(\Omega_r)}$	1	ζ_r

Table 2(a) Comparison and validation of results for an isotropic plates partially supported by an elastic foundation, with Motaghian et al. (2012) and Jahromi et al. (2013) at various B.Cs.

B.Cs	K_w	Present study		Jahromi *et al*. (2013)		Motaghian *et al*. (2012)	
		1st	2nd	1st	2nd	1st	2nd
SSSS	10	4.862	7.885	5.003	8.001	5.003	8.001
	1000	5.265	8.086	5.372	8.149	5.310	8.130
CSSS	10	5.118	8.745	5.239	8.729	5.279	8.880
	1000	5.519	8.714	5.621	8.883	5.604	9.013
CSCS	10	5.440	9.470	5.551	9.585	5.658	9.982
	1000	5.805	9.931	5.915	9.737	5.958	10.11

Table 2(b). Comparison and validation of results for an isotropic CCCC plates partially supported by an elastic foundation, with Motaghian *et al*. (2012) and Nguyen *et al*. (2022)

K_w	Present study		Jahromi *et al*. (2013)		Motaghian *et al*. (2012)	
	1st	2nd	1st	2nd	1st	2nd
10	10.04	13.09	10.03	13.12	10.29	13.35
1000	10.24	13.25	10.22	13.23	10.48	13.45

Table 3 Validation of The first natural frequencies (Hz) of SSSS sandwich plate with auxetic core made of Al with different values of β_1, θ and foundation stiffness, with Tran *et al*. (2020)

Substrate (K_1, K_2) (10^9 Pa/m, 10^9 Pa·m)	β_1	Tran *et al*. (2020)		Present study	
		Θ =10°	Θ =35°	Θ =10°	Θ =35°
without (0,0)	1	151.61	149.78	149.95	148.16
	2	152.17	151.71	150.50	150.05
	4	152.41	152.20	150.73	150.53
Winkler (0.1,0)	1	197.43	195.04	194.76	192.42
	2	198.16	197.56	195.47	194.88
	4	198.47	198.20	195.78	195.51
Pasternak (0,0.05)	1	250.34	247.31	246.37	243.41
	2	251.27	250.51	247.27	246.53
	4	251.67	251.32	247.66	247.32
Winkler Pasternak (0.1,0.05)	1	280.47	277.06	275.70	272.39
	2	281.51	280.66	276.72	275.88
	4	281.97	281.57	277.16	276.78

of Tran *et al*. (2020) with h_c/h_f=1.5, h=0.1m, a/h=20, β_3=0.01385. It can be seen that when the EF parameters increase, natural frequencies of plate increase. Also, results show the EF parameters make the plate become stiffener.

5.2 Numerical results

In this subsection, the frequency analysis of the sandwich plate with auxetic core and FG face layers, resting on PSEF,

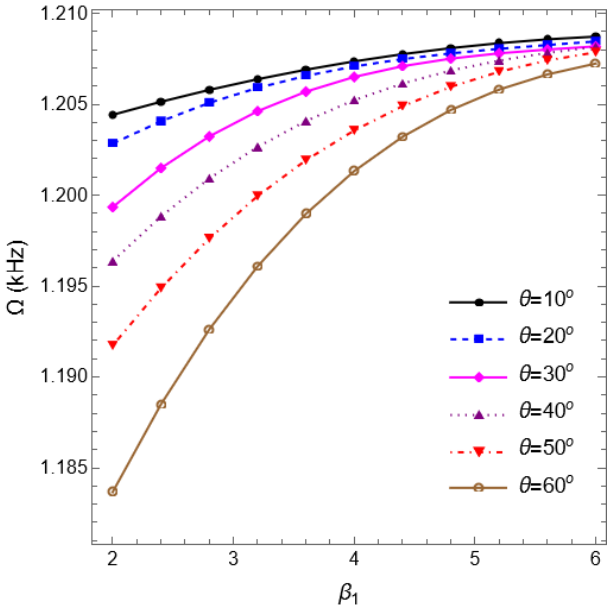

Fig. 4 Variation of the natural frequencies as a function of the auxetic layer's aspect ratio, at different inclined angle of the auxetic core

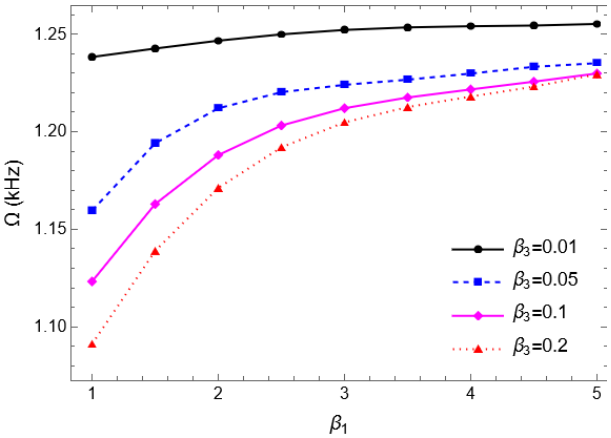

Fig. 5 Variation of the frequencies as a function of the auxetic layer's aspect ratio at various thickness of the walls in the auxetic core

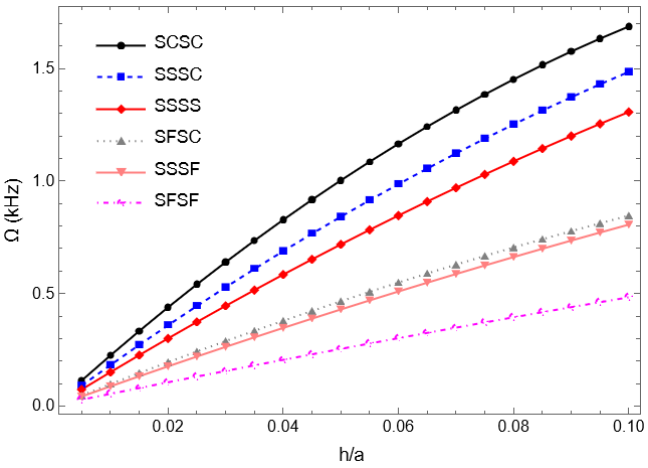

Fig. 6 Variation of Fundamental frequency of square plate as a function of thickness to length ratio at various BCs

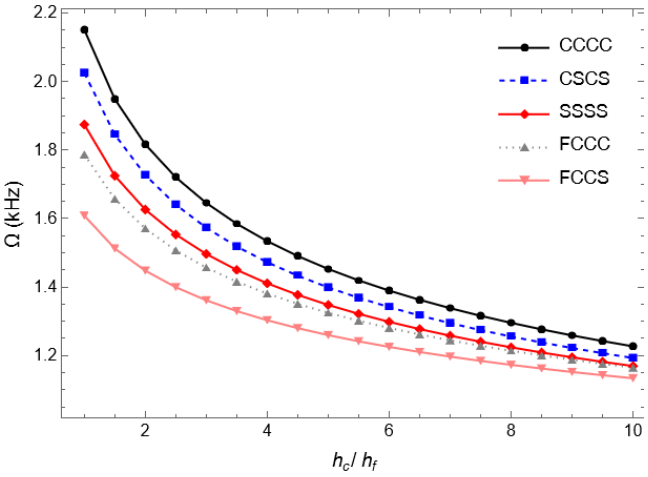

Fig. 7 Variation of fundamental frequency of sandwich plate versus core to face thickness ratio at various boundary conditions

and in thermal medium is examined with respect to the parameters of temperature rise, FGM index, Winkler coefficient and type of elastic foundation, core to face thickness ratio and geometrical features of auxetic core (θ, β_1 and β_3). The core and Face layers are made of stainless-steel metal (SUS304) and silicon–nitride ceramic (Si_3N_3). The Young's modulus, and the density of each material are supposed to be E_M = 208GPa, v_M = 0.3, and ρ_M = 8166 kg⁄m^3 of SUS304 and E_C = 322GPa, v_C = 0.3, ρ_C = 2370 kg⁄m^3 of Si_3N_3.

Fig. 4 illustrates how natural frequencies of plate depend on the aspect ratio of the cells in the auxetic core (β_1) and the inclined angle (θ). Increasing the inclined angle raises the number of cells and density, leading to various effects on the stiffness coefficients and increased inertia, which decreases the natural frequencies. The increase of parameter θ leads the unit cell's struts to become more inclined, and reducing their effective length, resulting in fewer resistance to deformation and softening the core, which causes a reduction in the natural frequency. Besides, Increasing β_1 parameter reduces the number of cells and density of core, causing changes in stiffness that ultimately raise the natural frequencies.

Fig. 5 investigates the dependency of the natural frequencies on the thickness of the walls of the cells in the auxetic core (β_3). By increasing the β_3 parameter, both density and elastic moduli increased based on Fig. 2 . As shown in Fig. 5, the natural frequencies decline with an increase in the thickness of the walls of the cells. Thus, as the thickness of the cells walls rised, the rate of density increase is exceeds than the increase rate in the elastic moduli.

Variation of Fundamental frequency of square plate versus the thickness to length ratio of plate have been plotted in Fig. 6 at various boundary conditions. Based on Fig. 6, higher limitations of deformation on boundary conditions causing rise in natural frequencies. Consequently, we can sort the boundary conditions in descendent order as SCSC, SSSC, SSSS, SFSC, SSSF and SFSF. Besides, Fig. 6

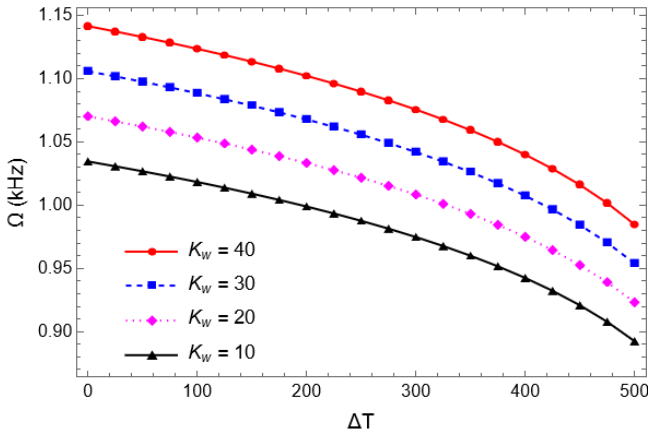

Fig. 8 Variation of fundamental frequency of CCCF sandwich plate versus temperature rise at different coefficients of EF for various Winkler Spring coefficients

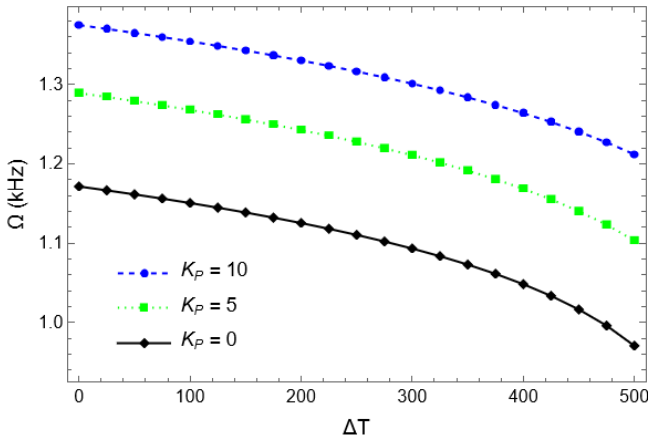

Fig. 9 Variation of fundamental frequency of CCCF sandwich plate versus temperature rise at different coefficients of EF for various Pasternak coefficients

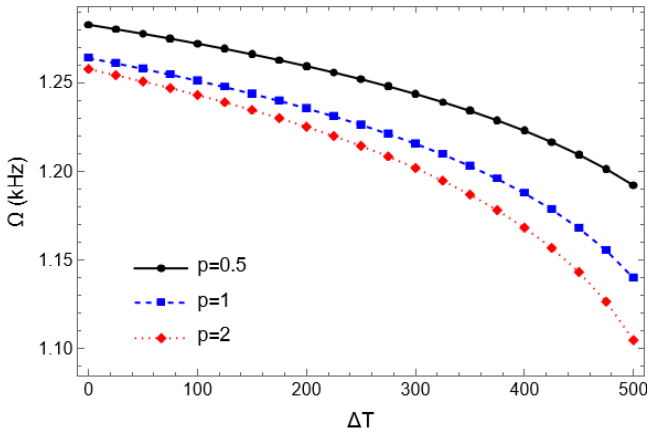

Fig. 10 Variation of fundamental frequency of SSSC sandwich plate versus temperature rise at various power indices of FGM faces

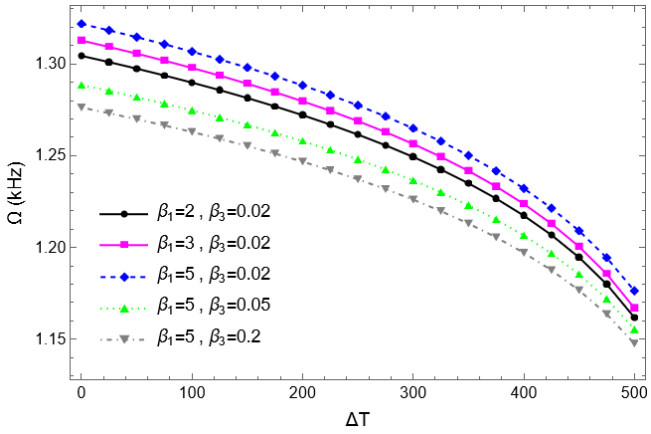

Fig. 11 Variation of the first natural frequency of the plate versus the temperature rise (ΔT) for diverse combinations of (β_1, θ)

shows that the natural frequencies rises by increasing the total thickness of sandwich plate.

Based on Fig. 7, it is observed that decreasing the core-to-FG face sheet thickness ratio (h_c/h_{fg}) leads to higher natural frequency. By reducing the h_c/h_{fg} ratio (an increase in the thickness of the FG layer and a decrease in the thickness of the core layer); since the stiffness of the FG layer is considerably greater than that of the core layer.

Figs. 8 and 9 exhibit the variation of the first natural frequency of the plate versus the temperature rise (ΔT) in the range of 0-500 °C with the step 25°C at different Winkler and Pasternak coefficients of EF. As the temperature rises, the first frequency of sandwich plate decreases slowly. The Ω reduced as the ΔT increases, while the rate of the decline is high at high temperature changes. The cause for this reduction in the frequency is the decrease in the structure's stiffness, due to compressive in-plane force created by increasing temperature. Based on Figs. 8 and 9, increasing both Winkler and Pasternak coefficients of foundation leads to enhancing the system's rigidity, and cause to rise of the natural frequencies.

Fig. 10 demonstrate the variation of the fundamental frequency versus temperature rise for three different power indices of FGM faces. Based on the Fig. 10, reducing the power indices and metallic phase in FGM face layers leads the rigidity to enhance, and it caused increasing in natural frequency. As can be seen, the natural frequency increased with increasing ceramic's volume fraction value. Enhancing the natural frequency is credited to the higher stiffness property of Si_3N_3 compared to SUS304. In addition, the thermal stress resultant of the plate increased with increasing metallic's volume fraction, and a substantial decrease in the natural frequency happened.

Fig. 11 displays the influences of the temperature rise, β_1 and β_3 on the frequencies of first mode in the sandwich plate. As shown in Fig. 11, the value of the fundamental frequency declines as both β_3 and ΔT increase. The cause for this reduction in the frequency is decreasing the elastic moduli of all the materials in the sandwich plate' layer with growing temperature, and reduce in the structure's stiffness. Additional cause for the reduction in the frequency is that the stiffness of the auxetic core growths as β_3 enhances, but the mass increases further than the stiffness.

To more examine the result of the PSEF on the fundamental frequency of the sandwich plate, two distributions of foundations are considered with assumptions

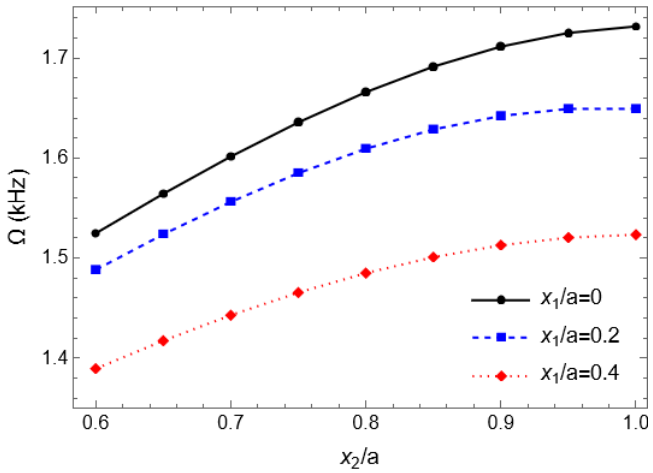

Fig. 12 Influence of arbitrarily distributed foundation geometric parameters on the fundamental frequency of the SCSC sandwich plate (Type 2)

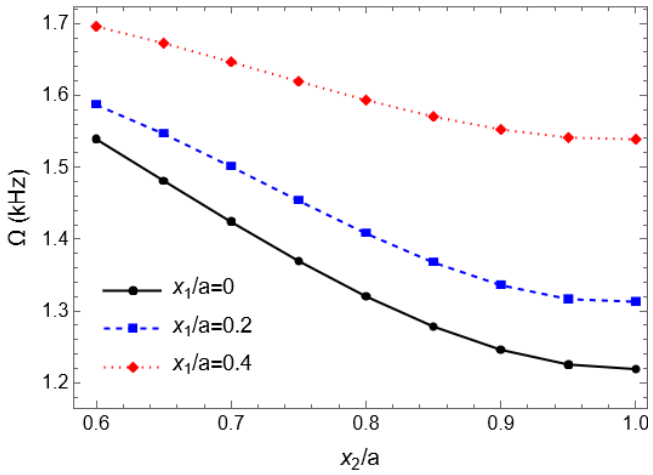

Fig. 13 Influence of arbitrarily distributed foundation geometric parameters on the fundamental frequency of the SCSC sandwich plate (Type 3)

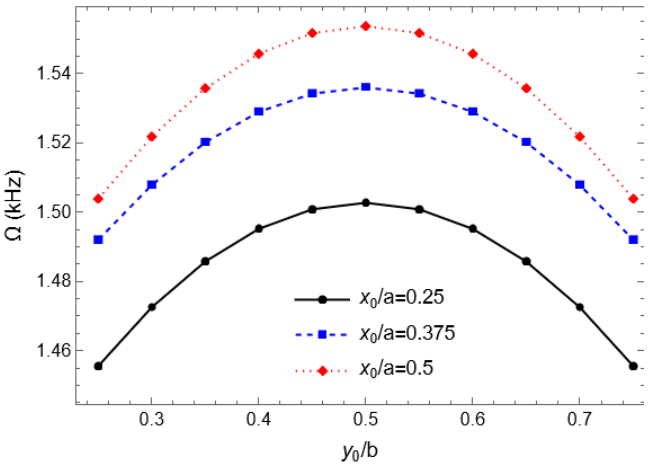

Fig. 14 Influence of the location of the PSEF on the fundamental frequency of the SCSC sandwich plate (Type 2)

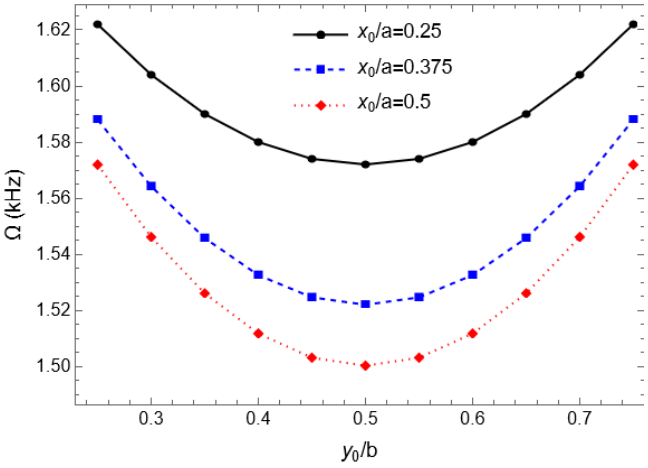

Fig. 15 Influence of the location of the PSEF on the fundamental frequency of the SCSC sandwich plate (Type 3)

y_1 = x_1, and y_2 =x_2. Figs. 12 and 13 give the effect of PSEF's geometric constraints on the fundamental frequency. As can be seen from Fig. 12, for Type 2, the fundamental frequency of the sandwich plate increases as parameter x_1/a reduces. The fundamental frequency rises as the value of x_2/a growths.

In Fig. 13, Type 3 illustrates the reverse order, since as the value of x_1/a reduces, the overall area of PSEF Type 2 rises though the overall area of PSEF Type 3 declines. As the value of x_2/a parameter growth, the overall area of PSEF Type 2 rises whereas the over-all area of PSEF Type 3 reduces. When the entire area of the PSEF rises, the stiffness of the system enhances.

The influence of the PSEF position on the fundamental frequency of the sandwich plate is considered in Figs. 14 and Fig. 15 Considering two different types of PSEF and assume that the center's coordinates for the PSEF are (x_0, y_0) i.e. $x_0 = \frac{x_1+x_2}{2}$, $y_0 = \frac{y_1+y_2}{2}$; also, y_1=x_1 and y_2=x_2. The total area of PSEF Type 2 and Type 3 have been kept constant at values of ab/4 and 3ab/4, respectively; and the borders of both x_0/a and y_0/b are in [0.25-0.75] bond. Based on, these figures for PSEF Type 2, the value of the fundamental frequency rises and then declines as x_0/a growths, and enhances and then reduces as the amplitudes of y_0/b reduces. The result's trend has been reversed for PSEF type 3. For PSEF Type 2, the value of the fundamental frequency is highest if the foundation locates in the plate's center. For PSEF Type 3, the maximum value of frequency is obtained by inserting an empty space at all the four corners of the sandwich plate.

6. Conclusions

In the present study, the HSDT is used to analyses the free vibration characteristics of sandwich plate with auxetic core and FGM faces, subjected to thermal medium and resting on PSEF. Since the material properties of the NPR auxetic core layer vary based on the three geometric parameters (β_1, β_3, and θ); the effective material properties were examined, and then the natural frequencies of the sandwich plate were obtained. The main findings are as

following:

• The elastic modulus, density and NPR of the auxetic core can be adjusted using the three main parameters of cells including thickness, aspect ratio and inclined angle.

• By increasing the parameter θ, the resistance to deformation in the core layer's auxetic cells decline and the stiffness of plate decrease, thus the variations in stiffness and inertia of plate result in lower frequencies.

• Rising the parameter β_1 decreases the number of cells and reduces the core layer's density. Also, the variations in inertia and stiffness of plate result in higher frequencies.

• Adjusting the geometrical parameters of the auxetic core layer can be an effective tactic in modifying the vibration behaviour of sandwich plate.

• By growing the temperature, the plate stiffness reduces and the natural frequencies, decrease.

• Placing the PSEF nearer to the plate's center enhances the plate's fundamental frequency. Hence, the design must prioritize locating resilient foundations at the center.

• As the power indices of FGM layers enhances, the plate vibrates at higher frequencies.

The present study recommends a new outlook on how to modify the mechanical characteristics of sandwich plate with thick auxetic core. Its illustrations that by regulating the three main parameters of cells it is possible to have a significant influence on their elastic moduli, density and NPR. This paper highlights the opportunity of attractive auxetic materials for precise engineering applications by employing these characteristics, thus allowing the progress of advanced material designs with upgraded impact resistance, vibration damping, shape memory capabilities and proficiencies in various engineering fields, such as aerospace, automotive and biomedical engineering.

In the future, researchers could investigate more studies about the dynamic characteristics of structures with auxetic layers, specifically in response to unexpected stimuli like vibration and impact, and prepare valuable information for practical applications.

References

Abo-Dahab, S.M., Abouelregal, A.E. and Marin, M. (2020), "Generalized thermoelastic functionally graded on a thin slim strip non-gaussian laser beam", *Symmetry*, **12**(7), 1094. https://doi.org/10.3390/sym12071094.

Alibeigloo, A. and Alizadeh, M. (2015), "Static and free vibration analyses of functionally graded sandwich plates using state space differential quadrature method," *Eur. J. Mech.*, **54**, 252-266. https://doi.org/10.1016/j.euromechsol.2015.06.011.

Alnujaie, A., Daikh, A.A., Ghazwani, M.H., Assie, A.E. and Eltaher, M.A. (2024), "Size-dependent free vibration of coated functionally graded graphene reinforced nanoplates rested on viscoelastic medium", *Adv. Nano Res.*, **17**(2), 181-195. https://doi.org/10.12989/anr.2024.17.2.181.

Ameer, S.A., Abdul Hussein, A.H., Mahdi, M.H., Elsaid, F.G. and Tahouneh, V. (2024), "Free vibration analysis of trapezoidal Double Layered plates embedded with viscoelastic medium for general boundary conditions using differential quadrature method", *Steel Compos. Struct.*, **50**(4), 429-441. https://doi.org/10.12989/scs.2024.50.4.429.

Arefi, M. (2015), "Elastic solution of a curved beam made of functionally graded materials with different cross sections", *Steel and Composite Structures, An Int'l Journal*, **18**(3), 659-672. https://doi.org/10.12989/scs.2015.18.3.659.

Arshid, E., Khorasani, M., Soleimani-Javid, Z., Amir, S. and Tounsi, A. (2021), "Porosity-dependent vibration analysis of FG microplates embedded by polymeric nanocomposite patches considering hygrothermal effect via an innovative plate theory", *Eng. Comput.*, 4051-4072. https://doi.org/10.1007/s00366-021-01382-y.

Barka, M., Benrahou, K.H., Bakora, A. and Tounsi, A. (2016), "Thermal post-buckling behavior of imperfect temperature-dependent sandwich FGM plates resting on Pasternak elastic foundation", *Steel Compos. Struct.*, **22**(1), 91-112. https://doi.org/10.12989/scs.2016.22.1.091.

Bennai, R., Ait Atmane, H. and Tounsi, A. (2015), "A new higher-order shear and normal deformation theory for functionally graded sandwich beams", *Steel Compos. Struct.*, **19**(3), 521-546. https://doi.org/10.12989/scs.2015.19.3.521.

Bhatti, M.M., Marin, M., Ellahi, R., Fudulu, I.M. (2023), "Insight into the dynamics of EMHD hybrid nanofluid (ZnO/CuO-SA) flow through a pipe for geothermal energy applications", *J. Therm. Anal. Calorim.*, **148**(96), 14261-14273. https://doi.org/10.1007/s10973-023-12565-8.

Bouchafa, A., Bouiadjra, M.B., Houari, M.S.A. and Tounsi, A. (2015), "Thermal stresses and deflections of functionally graded sandwich plates using a new refined hyperbolic shear deformation theory", *Steel Compos. Struct.*, **18**(6), 1493-1515. https://doi.org/10.12989/scs.2015.18.6.1493.

Bouguenina, O., Belakhdar, K., Tounsi, A. and Bedia, E.A.A. (2015), "Numerical analysis of FGM plates with variable thickness subjected to thermal buckling", *Steel Compos. Struct.*, **19**(3), 679-695. https://doi.org/10.12989/scs.2015.19.3.679.

Bouafia, H., Chikh, A., Bousahla,A.A., Bourada, F., Heireche, H., Tounsi, A., Benrahou, K.H., Tounsi,A., Al-Zahrani, M.M. and Hussain, M. (2021), "Natural frequencies of FGM nanoplates embedded in an elastic medium", *Adv. Nano Res.*, **11**(3), 239-249. https://doi.org/10.12989/anr.2021.11.3.239.

Boutaleb, S., Benrahou, K.H., Bakora, A., Algarni, A., Bousahla, A.A., Tounsi, A., Tounsi, A. and Mahmoud, S.R. (2019), "Dynamic analysis of nanosize FG rectangular plates based on simple nonlocal quasi 3D HSDT", *Adv. Nano Res.*, **7**(3), 191-208. https://doi.org/10.12989/anr.2019.7.3.191.

Chowdhary, S., Tafesse, B., A. A. Babu and Muthukumaran, G. (2021), "Prediction of influences of MWCNT fillers on the vibration characteristics of laminated hybrid honeycomb core sandwich GFRP composite plate", *Mater. Today Proc.*, **47**, 6670-6675. https://doi.org/10.1016/j.matpr.2021.05.110.

Dai, Z., Jiang, Z., Zhang, L. and Habibi, M. (2021), "Frequency characteristics and sensitivity analysis of a size-dependent laminated nanoshell", *Adv. Nano Res.*, **10**(2), 175-189. https://doi.org/10.12989/anr.2021.10.2.175.

Daikh, A., Ahmed Houari, M.S. and Tounsi, A. (2019), "Buckling analysis of porous FGM sandwich nanoplates due to heat conduction via nonlocal strain gradient theory", *Eng. Res. Express*, **1**(1). https://doi.org/10.1088/2631-8695/ab38f9

Daikh, A. and Megueni, A. (2018), "Thermal buckling analysis of functionally graded sandwich plates", *J. Therm. Stresses*, **41**, 139-145. https://doi.org/10.1080/01495739.2017.1393644

Ebrahimi, F., Fardshad, R.E. and Mahesh, V. (2019), "Frequency response analysis of curved embedded magneto-electro-viscoelastic functionally graded nanobeams", *Adv. Nano Res.*, **7**(6), 391-403. https://doi.org/10.12989/anr.2019.7.6.391.

Ghaznavi, A. and Shariyat, M. (2019), "Stress and displacement analysis of thick sandwich plates with deformable auxetic cores using an enhanced third order global-local theory", *J. Solid Fluid Mech.*, 2019. https://doi.org/10.22044/jsfm.2019.8231.2868.

Ghorbanpour Arani, A., Baba Akbar Zarei, H. and Haghparast, E.

(2018), "Vibration response of viscoelastic sandwich plate with magnetorheological fluid core and functionally graded-piezoelectric nanocomposite face sheets", *J. Vib. Control*, **24**(21), 5169-5185. https://doi.org/10.1177/1077546317747501.

Ha, N.H., Tan, N.C., Ninh, D.G., Hung, N.C. and Dao, D.V. (2023), "Dynamical and chaotic analyses of single-variable-edge cylindrical panels made of sandwich auxetic honeycomb core layer in thermal environment", *Thin-Walled Struct*., **183**. https://doi.org/10.1016/j.tws.2022.110300.

Hatami, S., Zarei, M.J. and Asghari Pari, S.H. (2024), "An innovative approach for analyzing free vibration in functionally graded carbon nanotube sandwich plates", *Adv. Nano Res*., **17**(1), 19-32. https://doi.org/10.12989/anr.2024.17.1.019.

Hajmohammad, M.H., Kolahchi, R., Zarei, M.S. and Nouri, A.H. (2019), "Dynamic response of auxetic honeycomb plates integrated with agglomerated CNT-reinforced face sheets subjected to blast load based on visco-sinusoidal theory", *Int. J. Mech. Sci*., **154**, 391-401. https://doi.org/10.1016/j.ijmecsci.2019.02.008.

Hoang, V.N.V., Shi, P., Toledo, L. and Vu, H. (2024), "Thermal vibration analysis of FG-GPLRC doubly curved shells partially resting on Kerr foundation based on higher-order shear deformation theory", *Thin-Walled Struct*., **195**. https://doi.org/10.1016/j.tws.2023.111357.

Hosseini, S.M. and Zhang, C. (2018), "Elastodynamic and wave propagation analysis in a FG Graphene platelets-reinforced nanocomposite cylinder using a modified nonlinear micro-mechanical model", *Steel Compos. Struct*., **27**(3), 255-271. https://doi.org/10.12989/scs.2018.27.3.255.

Jafari, P. and Kiani, Y. (2021), "Free vibration of functionally graded graphene platelet reinforced plates: A quasi 3D shear and normal deformable plate model", *Compos. Struct*., **275**, 114409. https://doi.org/10.1016/j.compstruct.2021.114409.

Jahromi, H. N., Aghdam, M.M. and Fallah, A. (2013), "Free vibration analysis of Mindlin plates partially resting on Pasternak foundation", *Int. J. Mech. Sci*., **75**, 1-7. https://doi.org/10.1016/j.ijmecsci.2013.06.001.

Jung, W.Y., Han, S.C. and Park, W.T. (2016), "Four-variable refined plate theory for forced-vibration analysis of sigmoid functionally graded plates on elastic foundation," *Int. J. Mech. Sci*., 73-87. https://doi.org/10.1016/j.ijmecsci.2016.03.001.

Karimiasl, M. and Alibeigloo, A. (2022), "Nonlinear free and forced vibration analysis of sandwich cylindrical panel with auxetic core and GPLRC facing sheets in hygrothermal environment", *Thin-Walled Struct*., **175**, 109164. https://doi.org/10.1016/j.tws.2022.109164.

Karimiasl, M. and Alibeigloo, A. (2023), "Nonlinear bending and vibration analysis of sandwich plate with graphene reinforced micro composite facing sheets and auxetic honeycomb core in thermal environment", *Microsyst. Technol*., **29**(12), 1739-1755. https://doi.org/10.1007/s00542-023-05561-3.

Khadir, A.I., Daikh, A.A. and Eltaher, M.A. (2021), "Novel four-unknowns quasi 3D theory for bending, buckling and free vibration of functionally graded carbon nanotubes reinforced composite laminated nanoplates", *Adv. Nano Res*., **11**(6), 621-640. https://doi.org/10.12989/anr.2021.11.6.621.

Khoddami Maraghi, Z., Amir, S. and Arshid, E. (2022), "On the natural frequencies of smart circular plates with magneto-rheological fluid core embedded between magnetostrictive patches on Kerr elastic substance", *Mech. Based Des. Struct*., 1651-1668. https://doi.org/10.1080/15397734.2022.2156885.

Kim, Y. W. (2015), "Free vibration analysis of FGM cylindrical shell partially resting on Pasternak elastic foundation with an oblique edge", *Compos. Part B Eng*., **70**, 263-276. https://doi.org/10.1016/j.compositesb.2014.11.024.

Kormanikova, E., Sol, H., Gu, J., Kotrasova, K., Kabosova, L. and Sabol, P. (2025), "Calculation and measurement of material properties of laminated polymer composite", *Steel Compos. Struct*., **54**(3), 251-261. https://doi.org/10.12989/scs.2025.54.3.251.

Kumar, P. and Harsha, S.P. (2021), "Vibration response analysis of exponential functionally graded piezoelectric (EFGP) plate subjected to thermo-electro-mechanical load", *Compos. Struct*., **267**, 113901. https://doi.org/10.1016/j.compstruct.2021.113901.

Kumar, V., Singh, S.J., Saran, V.H. and Harsha, S.P. (2021), "Vibration characteristics of porous FGM plate with variable thickness resting on Pasternak's foundation", *Eur. J. Mech*., **85**, 104124. https://doi.org/10.1016/j.euromechflu.2021.104124.

Liu, Z., Zhu, K., Wen, X. and Kumar, A. (2024), "Nonlinear vibration analysis of FG porous shear deformable cylindrical shells covered by CNTs-reinforced nanocomposite layers considering neutral surface exact position", *Adv. Nano Res*., **17**(1), 61-73. https://doi.org/10.12989/anr.2024.17.1.061.

Luo, D., Zhong, Y., Xi, S. and Shi, Z. (2021), "Static, buckling, and free-vibration analysis of plain-woven composite plate with finite thickness using VAM-based equivalent model", *Thin-Walled Struct*., **169**, 108503. https://doi.org/10.1016/j.tws.2021.108503.

Marin, M., Abbas, I., Kumar, R. (2014), "Relaxed Saint-Venant principle for thermoelastic micropolar diffusion", *Struct. Eng. Mech*., **51**(4), 651-662. https://doi.org/10.12989/sem.2014.51.4.651

Marin, M. (2010), "Some estimates on vibrations in thermo-elasticity of dipolar bodies", *J. Vib. Control*, **16** (1), 33-47. https://doi.org/10.1177/1077546309103419.

Marin, M., Seadawy, A. Vlase, S. and Chirila, A. (2022) "On mixed problem in thermoelasticity of type III for Cosserat media", *J. Taibah Univ. Sci*., **16**(1), 1264-1274. https://doi.org/10.1080/16583655.2022.2160290.

Mohammed, A.M., Mohammed, B.A., Kadhom, H.K., Taki, A.G. and Tahouneh, V. (2024), "A semi-analytical study for vibration analysis of damaged core laminated cylindrical shell with functionally graded CNTs reinforced face sheets resting on a two-parameter elastic foundation", *Adv. Nano Res*., **17**(4), 301-313. https://doi.org/10.12989/anr.2024.17.4.301.

Moraveji Tabasi, H., Eskandari Jam, J., Malekzadeh Fard, K. and Heydari Beni, M. (2020), "Buckling and free vibration analysis of fiber metal-laminated plates resting on partial elastic foundation", *J. Appl. Comput. Mech*., **6**(1), 37-51. https://doi.org/10.22055/JACM.2019.28156.1489.

Motaghian, S., Mofid, M. and Akin, J. E. (2012), "On the free vibration response of rectangular plates, partially supported on elastic foundation", *Appl. Math. Model*., **36**(9), 4473-4482. https://doi.org/10.1016/j.apm.2011.11.076.

Namazinia, N., Alibeigloo, A. and Karimiasl, M. (2024), "Free vibration and static analysis of sandwich composite plate with auxetic core and GPLRC facing sheets in hygrothermal environment," *Forces Mech*., **15**, 100264. https://doi.org/10.1016/j.finmec.2024.100264.

Natarajan, S. and Manickam, G. (2012), "Bending and vibration of functionally graded material sandwich plates using an accurate theory", *Finite Elem. Anal. Des*., **57**, 32-42. https://doi.org/10.1016/j.finel.2012.03.006.

Nguyen, D.D. and Pham, C.H. (2018), "Nonlinear dynamic response and vibration of sandwich composite plates with negative Poisson's ratio in auxetic honeycombs", *J. Sandw. Struct. Mater*., **20**(6), 692-717. https://doi.org/10.1177/1099636216674729.

Nguyen, P.C., Pham, Q.H., Tran, T.T. and Nguyen-Thoi, T. (2022), "Effects of partially supported elastic foundation on free vibration of FGP plates using ES-MITC3 elements", *Ain Shams Eng. J.*, **13**(3), 101615. https://doi.org/10.1016/j.asej.2021.10.010.

Park, W.T., Han, S.C., Jung, W.Y. and Lee, W.H. (2016),

"Dynamic instability analysis for S-FGM plates embedded in Pasternak elastic medium using the modified couple stress theory", *Steel Compos. Struct.*, **22**(6), 1239-1259. https://doi.org/10.12989/scs.2016.22.6.1239.

Pham, H.C., Pham, M. P., Hoang, T.T., Duong, T.M. and Nguyen, D.D. (2020), "Static bending analysis of auxetic plate by FEM and a new third-order shear deformation plate theory", *VNU J. Sci. Nat. Sci. Technol.*, **36**(1). https://doi.org/10.25073/2588-1140/vnunst.5000.

Praveen A.P., Rajamohan, V., Arumugam, A.B. and Mathew, A.T. (2020), "Vibration analysis of a multifunctional hybrid composite honeycomb sandwich plate", *J. Sandw. Struct. Mater.*, **22**(8), 2818-2860. https://doi.org/10.1177/1099636218820764.

Qi, C., Remennikov, A., Pei, L.Z., Yang, S., Yu, Z.H. and Ngo, T.D. (2017), "Impact and close-in blast response of auxetic honeycomb-cored sandwich panels: experimental tests and numerical simulations", *Compos. Struct.*, **180**, 161-178. https://doi.org/10.1016/j.compstruct.2017.08.020.

Sarvestani, H.Y., Akbarzadeh, A.H., Niknam, H. and Hermenean, K. (2018), "3D printed architected polymeric sandwich panels: Energy absorption and structural performance", *Compos. Struct.*, **200**, 886-909. https://doi.org/10.1016/j.compstruct.2018.04.002.

Shahbaztabar, A. and Arteshyar, K. (2019), "Buckling analysis of functionally graded plates partially resting on elastic foundation using the differential quadrature element method", *Acta Mech. Sin.*, **35**, 174-189. https://doi.org/10.1007/s10409-018-0796-6.

Shen, H.S., Xiang, Y. and Lin, F. (2017), "Nonlinear vibration of functionally graded graphene-reinforced composite laminated plates in thermal environments", *Comput. Methods Appl. Mech. Eng.*, **319**, 175-193. https://doi.org/10.1016/j.cma.2017.02.029.

Shen, X., Li, T., Xu, L., Kiarasi, F., Babaei, M. and Asemi, K. (2024), "Free vibration analysis of FG porous spherical cap reinforced by graphene platelet resting on Winkler foundation", *Adv. Nano Res.*, **16**(1), 11-26. https://doi.org/10.12989/anr.2024.16.1.011.

Singh, S.J. and Harsha, S.P. (2021), "Free vibration analysis of sandwich plate with honeycomb core and FGM face sheets", *Advances in Systems Engineering: Select Proceedings of NSC 2019, Springer*, 905-917. https://doi.org/10.1007/978-981-15-8025-3_85.

Tahouneh, V., Naei, M.H., Mosavi Mashhadi, M. (2019), "Using IGA and trimming approaches for vibrational analysis of L-shape graphene sheets via nonlocal elasticity theory", *Steel Compos. Struct.*, **33**(5), 717-727. https://doi.org/10.12989/scs.2019.33.5.717.

Tahouneh, V., Naei, M.H., Mosavi Mashhadi, M. (2020), "Influence of vacancy defects on vibration analysis of graphene sheets applying isogeometric method: Molecular and continuum approaches", *Steel Compos. Struct.*, **34**(2), 261-277. https://doi.org/10.12989/scs.2020.34.2.261.

Tahouneh, V. (2017), "Vibration and mode shape analysis of sandwich panel with MWCNTs FG-reinforcement core", *Steel Compos. Struct.*, **25**(3), 347-360. https://doi.org/10.12989/scs.2017.25.3.347.

Thang, N.T., Van Long, N., Tu, T.M., Nam, N.H. and Anh, M.C. (2022), "Navier solution for static and free vibration analysis of sandwich plate with auxetic honeycomb core resting on Pasternak elastic foundation", *J. Sci. Technol. Civ. Eng. (JSTCE)-HUCE*, **16**(3), 18-28. https://doi.org/10.31814/stce.huce(nuce)2022-16(3)-02.

Tornabene, F. (2009), "Free vibration analysis of functionally graded conical cylindrical shell and annular plate structures with a four-parameter power-law distribution", *Comput. Meth. Appl. Mech. Eng.*, **198**(37), 2911-2935. https://doi.org/10.1016/j.cma.2009.04.011.

Tornabene, F. and Ceruti, A. (2013), "Mixed static and dynamic optimization of four-parameter functionally graded completely doubly curved and degenerate shells and panels using GDQ method", *Math. Probl. Eng.*, 1-33. https://doi.org/10.1155/2013/867079.

Tornabene, F., Fantuzzi, N. and Bacciocchi, M. (2014), "Free vibrations of free-form doubly curved shells made of functionally graded materials using higher-order equivalent single layer theories", *Compos. Part B*, **67**(1), 490-509. https://doi.org/10.1016/j.compositesb.2014.08.012.

Tran, T.T., Pham, Q.H., Nguyen-Thoi, T. and Van Tran, T. (2020), "Dynamic analysis of sandwich auxetic honeycomb plates subjected to moving oscillator load on elastic foundation", *Adv. Mater. Sci. Eng.*, 6309130. https://doi.org/10.1155/2020/6309130.

Wang, C., Cai, L., Gao, M., Jin, L., Sun, L., Tang, X., Shi, G., Zheng, X. and Guo, C. (2023), "Manufacturing of membrane acoustical metamaterials for low frequency noise reduction and control: A review", *Mech. Adv. Mater. Struct.*, 7008-7023. https://doi.org/10.1080/15376494.2023.2242363.

Wang, L., Mohsin, H.F., Bains, P.S., Sharma, R. and Bohlooli, N. (2025), "Vibration analysis of elastically supported sandwich beam with damaged core and functionally graded face sheets", *Steel Compos. Struct.*, **54**(1), 71-83. https://doi.org/10.12989/scs.2025.54.1.071.

Wang, T., Qin, Q., Wang, M., Yu, W., Wang, J., Zhang, J. and Wang, T.J. (2017), "Blast response of geometrically asymmetric metal honeycomb sandwich plate: Experimental and theoretical investigations", *Int. J. Impact Eng.*, **105**, 24-38. https://doi.org/ 10.1016/j.ijimpeng.2016.10.009.

Yadav, A.K., Carrera, E., Marin, M. and Othman M.I.A. (2024), "Reflection of hygrothermal waves in a Nonlocal Theory of coupled thermo-elasticity", *Mech. Adv. Mater. Struct.*, **31**(5), 1083-1096. https://doi.org/10.1080/15376494.2022.2130484.

Yuanlong, W., Wanzhong, Z., Guan, Z. and Chunyan, W. (2018), "Analysis and parametric optimization of a novel sandwich panel with double-V auxetic structure core under air blast loading", *Int. J. Mech. Sci.*, **142**, 245-254. https://doi.org/10.1016/j.ijmecsci.2018.05.001.

Zhu, X., Zhang, J., Zhang, W. and Chen, J. (2019), "Vibration frequencies and energies of an auxetic honeycomb sandwich plate", *Mech. Adv. Mater. Struct.*, **26**(23), 1951-1957. https://doi.org/10.1080/15376494.2018.1455933.

CC

Appendix A

The domain of integral of Eq. (13) for different types of PSEF are described as follows:

$$\text{(type 1): } \delta U_F = \int_0^a \int_0^b \left[\mathrm{k}_w (w_b + w_s)\delta(w_b + w_s) + \mathrm{k}_p \begin{pmatrix} \frac{\partial (w_b+w_s)}{\partial \zeta}\frac{\partial \delta(w_b+w_s)}{\partial \zeta} + \\ \frac{\partial (w_b+w_s)}{\partial \eta}\frac{\partial \delta(w_b+w_s)}{\partial \eta} \end{pmatrix} \right] d\zeta d\eta \tag{A1}$$

$$\text{(type 2): } \delta U_F = \int_{x_1}^{x_2} \int_{y_1}^{y_2} \left[\mathrm{k}_w (w_b + w_s)\delta(w_b + w_s) + \mathrm{k}_p \begin{pmatrix} \frac{\partial (w_b+w_s)}{\partial \zeta}\frac{\partial \delta(w_b+w_s)}{\partial \zeta} + \\ \frac{\partial (w_b+w_s)}{\partial \eta}\frac{\partial \delta(w_b+w_s)}{\partial \eta} \end{pmatrix} \right] d\zeta d\eta \tag{A2}$$

$$\begin{aligned} \text{(type3): } \delta U_F = {} & \int_0^{x_1} \int_0^b \left[\mathrm{k}_w (w_b + w_s)\delta(w_b + w_s) + \mathrm{k}_p \begin{pmatrix} \frac{\partial (w_b+w_s)}{\partial \zeta}\frac{\partial \delta(w_b+w_s)}{\partial \zeta} + \\ \frac{\partial (w_b+w_s)}{\partial \eta}\frac{\partial \delta(w_b+w_s)}{\partial \eta} \end{pmatrix} \right] d\zeta d\eta + \int_{x_1}^{x_2} \int_0^{y_1} \left[\mathrm{k}_w (w_b + \right. \\ & w_s)\delta(w_b + w_s) + \mathrm{k}_p \begin{pmatrix} \frac{\partial (w_b+w_s)}{\partial \zeta}\frac{\partial \delta(w_b+w_s)}{\partial \zeta} + \\ \frac{\partial (w_b+w_s)}{\partial \eta}\frac{\partial \delta(w_b+w_s)}{\partial \eta} \end{pmatrix} \Big] d\zeta d\eta + \int_{x_1}^{x_2} \int_{y_2}^{b} \left[\mathrm{k}_w (w_b + w_s)\delta(w_b + w_s) + \right. \\ & \left. \mathrm{k}_p \begin{pmatrix} \frac{\partial (w_b+w_s)}{\partial \zeta}\frac{\partial \delta(w_b+w_s)}{\partial \zeta} + \\ \frac{\partial (w_b+w_s)}{\partial \eta}\frac{\partial \delta(w_b+w_s)}{\partial \eta} \end{pmatrix} \right] d\zeta d\eta + \int_{x_2}^{a} \int_0^b \left[\mathrm{k}_w (w_b + w_s)\delta(w_b + w_s) + \mathrm{k}_p \begin{pmatrix} \frac{\partial (w_b+w_s)}{\partial \zeta}\frac{\partial \delta(w_b+w_s)}{\partial \zeta} + \\ \frac{\partial (w_b+w_s)}{\partial \eta}\frac{\partial \delta(w_b+w_s)}{\partial \eta} \end{pmatrix} \right] d\zeta d\eta \end{aligned} \tag{A3}$$

Appendix B

$$\begin{Bmatrix} N_x \\ N_y \\ N_{xy} \end{Bmatrix} = \left\{ \begin{pmatrix} A_{11} & A_{12} & 0 \\ A_{12} & A_{22} & 0 \\ 0 & 0 & A_{66} \end{pmatrix} \begin{Bmatrix} \frac{\partial u}{\partial x} \\ \frac{\partial v}{\partial y} \\ \frac{\partial u}{\partial y} + \frac{\partial v}{\partial x} \end{Bmatrix} + \begin{pmatrix} B_{11} & B_{12} & 0 \\ B_{12} & B_{22} & 0 \\ 0 & 0 & B_{66} \end{pmatrix} \begin{Bmatrix} -\frac{\partial^2 w_b}{\partial x^2} \\ -\frac{\partial^2 w_b}{\partial y^2} \\ -2\frac{\partial^2 w_b}{\partial x \partial y} \end{Bmatrix} + \begin{pmatrix} B_{11}^s & B_{12}^s & 0 \\ B_{12}^s & B_{22}^s & 0 \\ 0 & 0 & B_{66}^s \end{pmatrix} \begin{Bmatrix} -\frac{\partial^2 w_s}{\partial x^2} \\ -\frac{\partial^2 w_s}{\partial y^2} \\ -2\frac{\partial^2 w_s}{\partial x \partial y} \end{Bmatrix} \right\} \tag{B1}$$

$$\begin{Bmatrix} M_x^s \\ M_y^s \\ M_{xy}^s \end{Bmatrix} = \left\{ \begin{pmatrix} B_{11}^s & B_{12}^s & 0 \\ B_{12}^s & B_{22}^s & 0 \\ 0 & 0 & B_{66}^s \end{pmatrix} \begin{Bmatrix} \frac{\partial u}{\partial x} \\ \frac{\partial v}{\partial y} \\ \frac{\partial u}{\partial y} + \frac{\partial v}{\partial x} \end{Bmatrix} + \begin{pmatrix} D_{11}^s & D_{12}^s & 0 \\ D_{12}^s & D_{22}^s & 0 \\ 0 & 0 & D_{66}^s \end{pmatrix} \begin{Bmatrix} -\frac{\partial^2 w_b}{\partial x^2} \\ -\frac{\partial^2 w_b}{\partial y^2} \\ -2\frac{\partial^2 w_b}{\partial x \partial y} \end{Bmatrix} + \begin{pmatrix} H_{11}^s & H_{12}^s & 0 \\ H_{12}^s & H_{22}^s & 0 \\ 0 & 0 & H_{66}^s \end{pmatrix} \begin{Bmatrix} -\frac{\partial^2 w_s}{\partial x^2} \\ -\frac{\partial^2 w_s}{\partial y^2} \\ -2\frac{\partial^2 w_s}{\partial x \partial y} \end{Bmatrix} \right\} \tag{B2}$$

$$\begin{Bmatrix} M_x^b \\ M_y^b \\ M_{xy}^b \end{Bmatrix} = \left\{ \begin{pmatrix} B_{11} & B_{12} & 0 \\ B_{12} & B_{22} & 0 \\ 0 & 0 & B_{66} \end{pmatrix} \begin{Bmatrix} \dfrac{\partial u}{\partial x} \\ \dfrac{\partial v}{\partial y} \\ \dfrac{\partial u}{\partial y} + \dfrac{\partial v}{\partial x} \end{Bmatrix} + \begin{pmatrix} D_{11} & D_{12} & 0 \\ D_{12} & D_{22} & 0 \\ 0 & 0 & D_{66} \end{pmatrix} \begin{Bmatrix} -\dfrac{\partial^2 w_b}{\partial x^2} \\ -\dfrac{\partial^2 w_b}{\partial y^2} \\ -2\dfrac{\partial^2 w_b}{\partial x \partial y} \end{Bmatrix} + \begin{pmatrix} D_{11}^s & D_{12}^s & 0 \\ D_{12}^s & D_{22}^s & 0 \\ 0 & 0 & D_{66}^s \end{pmatrix} \begin{Bmatrix} -\dfrac{\partial^2 w_s}{\partial x^2} \\ -\dfrac{\partial^2 w_s}{\partial y^2} \\ -2\dfrac{\partial^2 w_s}{\partial x \partial y} \end{Bmatrix} \right\}. \tag{B3}$$

$$\begin{Bmatrix} Q_{xz} \\ Q_{yz} \end{Bmatrix} = \left\{ \begin{pmatrix} A_{44}^s & 0 \\ 0 & A_{55}^s \end{pmatrix} \begin{Bmatrix} \dfrac{\partial w_s}{\partial x} \\ \dfrac{\partial w_s}{\partial y} \end{Bmatrix} - A_{15}^e \begin{Bmatrix} \dfrac{\partial \varphi}{\partial x} \\ \dfrac{\partial \varphi}{\partial y} \end{Bmatrix} \right\} \tag{B4}$$

In which the expressed cross-sectional rigidities are:

$$\begin{Bmatrix} A_{11}, B_{11}, B_{11}^s, D_{11}, D_{11}^s, H_{11}^s \\ A_{12}, B_{12}, B_{12}^s, D_{12}, D_{12}^s, H_{12}^s \\ A_{66}, B_{66}, B_{66}^s, D_{66}, D_{66}^s, H_{66}^s \end{Bmatrix} = \int_{\frac{-h_{fg}-h_c}{2}}^{\frac{h_{fg}+h_c}{2}} \begin{Bmatrix} \tilde{c}_{11} \\ \tilde{c}_{12} \\ \tilde{c}_{66} \end{Bmatrix} (1, z, f, z^2, zf, f^2) dz,$$
$$A_{44}^s = A_{55}^s = \int_{-h_{fg}-h_c/2}^{h_{fg}+h_c/2} \tilde{c}_{55} g^2 dz \tag{B5}$$